Supplementary Information

Supplementary Methods

MRI data acquisition. At the neonatal timepoint, after feeding, the infant was swaddled and positioned in a head-stabilizing vacuum fix wrap. A nurse familiar with neonate transport and resuscitation was present at all MRI scans. Heart rate and blood oxygenation were measured continuously throughout all scans, and infants were monitored visually via video. Based on visual monitoring through a camera, infants slept through scans as indicated by eye closure and minimal movements. Imaging was performed without sedating medications using a Siemens 3T Prisma scanner and 64-channel head coil. A T2-weighted image (sagittal, 208 slices, 0.8mm isotropic resolution, echo time [TE] = 563 ms, repetition time [TR] = 3200 ms) was collected. For the resting-state fMRI, functional imaging was performed using a blood-oxygen-level dependent (BOLD) gradient-recalled echo-planar multiband (MB) sequence (72 slices, 2.0-mm isotropic resolution, TE = 37 ms, TR = 800 ms, MB factor = 8). Scans were collected in both the anterior-posterior (AP) and posterior-anterior (PA) direction; a typical session included two AP scans and two PA scans. Each scan was 420 frames, which is 5.6 min in length.

At the toddler (two- and three-year) timepoints, during naptime or after bedtime, the child was allowed to fall asleep naturally in the presence of the parent. The child was then positioned in the scanner with the use of custom head padding and weighted cushions and blankets. Toddlers were monitored visually via video; based on video, toddlers slept through scans as indicated by eye closure and minimal movements. Imaging was performed without sedating medications using a Siemens 3T Prisma scanner and 64-channel head coil. A T1-weighted image (sagittal, 208 slices, 0.8mm isotropic resolution, TR = 2400 ms, TE = 2.22 ms) was collected. For the resting-state fMRI, functional imaging was performed using an identical BOLD gradient-recalled echo-planar MB sequence (72 slices, 2.0-mm isotropic resolution, TE = 37 ms, TR = 800 ms, MB factor = 8). Scans were collected in the AP direction; the scans were 420 frames, which is 5.6 min in length.

Network analysis. Residual mean BOLD time series were extracted from a 333-region cortical parcellation[1], and we represented the functional connectivity matrix as a graph or network[2]. Regions were represented by network nodes, and the functional connectivity between region *i* and region *j* was represented by the network edge between node *i* and node *j*. We estimated the functional connectivity between any two brain regions by calculating the product-moment correlation coefficient *r* between the mean activity time series of region *i* and the mean activity time series of region *j*[3]. We used this encoding of the data as a network to produce an undirected, signed, and weighted adjacency matrix A. Correlations were subsequently *r*-to-*z* transformed. Because there is not yet consensus on the spatial layout of neonatal functional networks[4–10], we assigned nodes to 13 large-scale systems (also sometimes called “networks”) based on the definitions of functional systems derived in healthy adults[1].

Prior evidence has demonstrated that the maintenance of edge weights is critical for an accurate understanding of the underlying biology of neural systems[11,12], and work in applied

mathematics has demonstrated that graph-related calculations are markedly more robust in weighted graphs than in binary graphs[13]. In light of these two lines of evidence and recent work in the field developing methods sensitive to the topologies present in weak versus strong edges[14], we maintained all edge weights without thresholding and studied the full graph including both positive and negative correlations[15,16].

Measures of functional network architecture

System segregation. System segregation quantifies the difference in mean within-system connectivity and mean between-system connectivity as a proportion of within-system connectivity. Previous work has linked this measure to aging-related changes in brain networks and poorer cognitive ability across age[17,18]. In these analyses, we define system segregation as in [17], as:

$$\frac{\bar{a}_{within} - \bar{a}_{between}}{\bar{a}_{within}}$$

Where $\bar{a}_{within}$ is the mean edge weight between nodes within the same system and $\bar{a}_{between}$ is the mean edge weight between nodes of one system to all nodes in other systems. We assigned nodes to systems based on a 13-system partition[1]. Freely available MATLAB code from https://github.com/mychan24/system_matrix_tools was used to calculate system segregation.

Modularity. Statistics that quantify the modular structure of a network assess the extent to which a network's nodes can be subdivided into groups or modules characterized by strong, dense intramodular connectivity and weak, sparse intermodular connectivity. We considered the most commonly studied mesoscale organization—assortative community structure—that is commonly assessed by maximizing a modularity quality function[19,20]. Unlike system segregation, the modularity quality index is independent of a mapping of nodes to functional systems. Higher modularity is indicative of a more highly segregated network at the mesoscale. Our approach is built on the modularity quality function originally defined by[21] and subsequently extended to weighted and signed networks by various groups.

Specifically, we follow [14] by first letting the weight of a positive connection between nodes i and j be given by a_{ij}^{+} , the weight of a negative connection between nodes i and j be given by $a^{-}{}_{ij}$, and the strength of a node i, $s_i^{\pm} = \sum_j a^{\pm}_{ij}$, be given by the sum of the positive or negative j connection weights of i. We denote the chance expected within-module connection weights as e_{ij}^{+} for positive weights and e_{ij}^{-} for negative weights, where $e_{ij}^{\pm} = \frac{s_i^{\pm} s_j^{\pm}}{v^{\pm}}$. We let the total weight $v^{\pm} = \sum_{ij} a_{ij}^{\pm}$ be the sum of all positive or negative connection weights in the network. Then, the asymmetric generalization of the modularity quality index is given by:

$$Q^{*} = \frac{1}{v^{+}} \sum_{ij} \left(a_{ij}^{+} - e_{ij}^{+}\right) \delta_{M_i M_j} - \frac{1}{v^{+} + v^{-}} \sum_{ij} \left(a_{ij}^{-} - e_{ij}^{-}\right) \delta_{M_i M_j}$$

where M_i is the community to which node i is assigned, and M_j is the community to which node j is assigned. We use a Louvain-like locally greedy algorithm as a heuristic to maximize this modularity quality index subject to a partition M of nodes into communities. We ran the Louvain algorithm 100 times per network, and detected on average four (*M* = 3.76, *SD* = 0.51) communities using modularity maximization in our developmental sample.

*Clustering coefficient***.** To assess local network segregation, we used a commonly studied graph measure of local connectivity—the clustering coefficient— that is commonly interpreted as reflecting the capacity of the system for processing within the immediate neighborhood of a given network node[22–25]. We specifically used a formulation that was recently generalized to signed weighted networks[26,27]. This version is sensitive to nonredundancy in path information based on edge sign as well as edge weight and importantly distinguishes between positive triangles and negative triangles, which have distinct meanings in networks constructed from correlation matrices.

We let the functional connectivity network of a single participant be represented as the graph $G = (V, E)$, where V and E are the vertex and edge sets, respectively. We let a_{ij} be the weight associated with the edge $(i, j) \in V$, and define the weighted adjacency matrix of G as $A = [a_{ij}]$. The clustering coefficient of node i with neighbors j and q is given by:

$$C_i = \frac{\sum_{jq} \left(a_{ji} a_{iq} a_{jq}\right)}{\sum_{j \neq q} \left|a_{ji} a_{iq}\right|}$$

The clustering coefficient of the entire network was calculated as the average of the clustering coefficient across all nodes as follows:

$$C = \frac{1}{n} \sum_{i \in N} C_i$$

In this way, we obtained estimates of the regional and global clustering coefficient for each subject in the sample.

Participation coefficient. The participation coefficient is a measure of network integration that quantifies the diversity of a node's connections across communities, and has been linked in older children and adolescents to developmental changes in network segregation[28–30]. A node has a high participation coefficient when it is evenly and strongly connected to many different systems. In these analyses, we define the participation coefficient P_i of a node i as:

$$P_i = 1 - \sum_{k \in K} \left(\frac{a_{ik}}{s_i}\right)$$

where k is a system in a set K of systems, in this case defined by the *a priori* mapping of nodes to intrinsic functional systems, a_{ik} is the positive (negative) weight of edges between node i and nodes in system k, and s_i is the positive (negative) strength of node *i*. The participation coefficient was calculated separately on negative and positive weights[31].

As in our analyses of local segregation, the participation coefficient of the entire network was calculated as the average positive (negative) participation coefficient across all nodes as follows:

$$P = \frac{1}{n}\sum_{i \in N} P_i$$

The average positive and negative participation coefficient for each participant's network were averaged to obtain a global measure of network integration.

Supplementary Note 1

To ensure that the environmental associations with changes in cortical network segregation observed were robust to methodological variation and potential confounds, we performed five sensitivity analyses. The first sensitivity analysis is described in the main text. In the second sensitivity analysis, GAMMs were rerun with only participants who had full data at two or more timepoints (Supplementary Figure 1). In a third sensitivity analysis, we refit GAMMs including a measure of pre-censoring motion, rather than the post-censoring measure used in our main analyses (Supplementary Figure 2). Finally, we conducted several pre-registered follow-up analyses related to changes in disadvantage over time. We first examined the extent of changes in indicators of disadvantage, finding that there was little social mobility during the study period (Supplementary Figure 3). Then, we reran GAMMs including the disadvantage factor calculated at Y1 and Y2, rather than at birth.

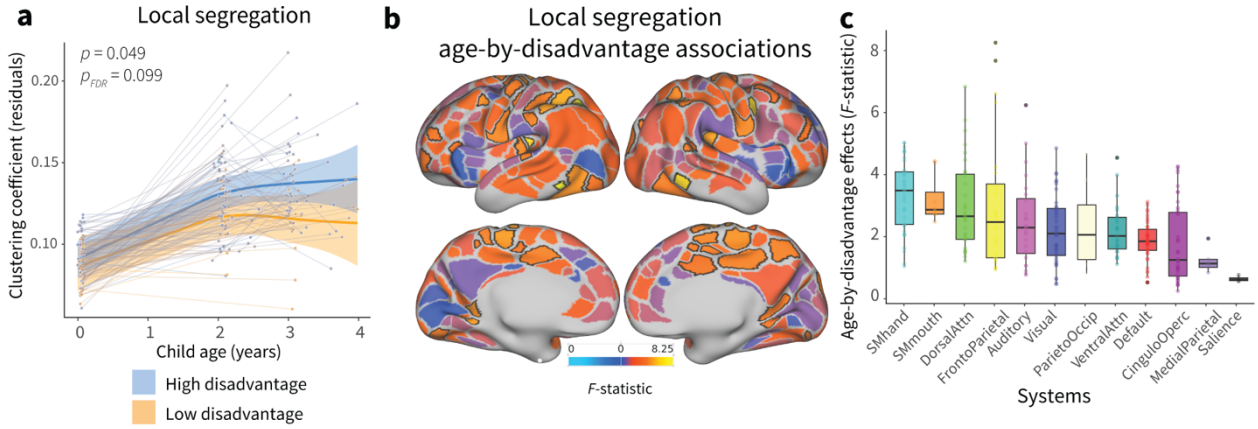

Supplementary Figure 1. Associations between the early environment and developmental increases in cortical network segregation, including only participants with two or more timepoints of data. **a,** Prenatal disadvantage moderates trajectories of local cortical network segregation. Trajectories represent the GAMM-predicted segregation values with a 95% credible interval band. **b,** The heterogenous patterning of the magnitude of age-by-disadvantage effects (F-statistic) on local segregation is shown on the cortical surface. Regions that show significant age-by-disadvantage effects passing FDR correction at $p_{FDR} < 0.05$ are outlined in black. **c,** Disadvantage associations with developmental increases in local segregation are enriched in sensorimotor systems. Boxplots show the magnitude of age-by-disadvantage effects; each point is an individual parcel (n = 286 parcels, excluding parcels with system assignment None). Boxplots show median and 25%-75% interquartile range; whiskers extend to 1.5 * interquartile range, points outside are shown as outliers.

We additionally verified whether results are robust to only including participants with two or more timepoints of data collected. When limiting our sample to this subsample, due to a decrease in sample size (n = 105 unique participants), we have less power to detect significant effects, however, we still expect to observe effects in the same direction as those observed in our primary analyses. Global segregation ($F_{s(agexSES)} = 2.35$, $p = 0.098$, $p_{FDR} = 0.131$), meso-scale segregation ($F_{s(agexSES)} = 9.24$, $p < 0.001$, $p_{FDR} < 0.001$), and local segregation

(Supplementary Figure 1a, $F_{s(agexSES)}$ = 2.78, p = 0.049, p_{FDR} = 0.100) show similar patterns of interactions, such that infants and toddlers exposed to greater prenatal disadvantage show a faster increase in cortical network segregation than infants and toddlers with less disadvantage exposure. We did not find evidence for moderating associations of disadvantage with developmental changes in network integration ($F_{s(agexSES)}$ = 0.001, p = 0.999, p_{FDR} = 0.999). The magnitude of disadvantage associations with developmental increases in local segregation differed across functional systems, with the strongest associations found in somatomotor-hand, somatomotor-mouth, dorsal attention, and frontoparietal systems (Supplementary Figure 1c).

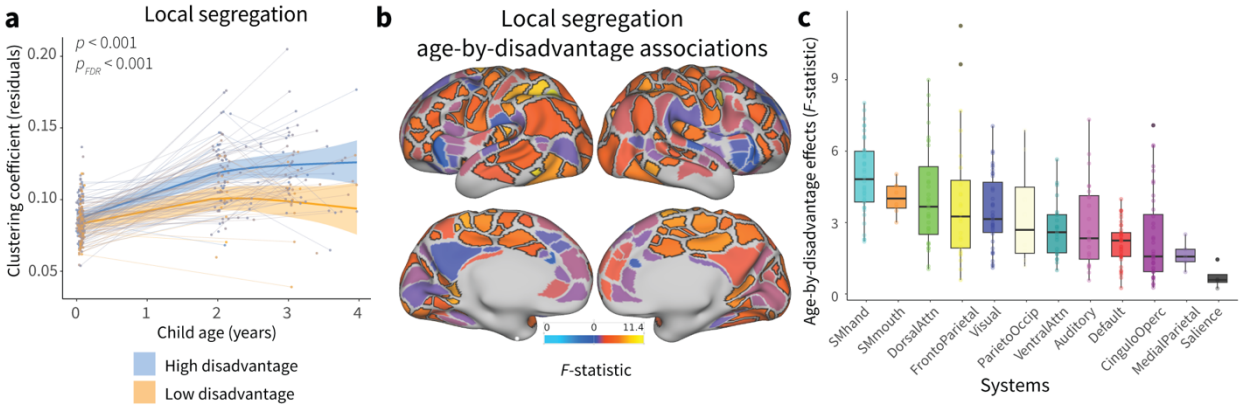

Supplementary Figure 2. Associations between the early environment and developmental increases in cortical network segregation, controlling for pre-censoring motion. **a,** Prenatal disadvantage moderates trajectories of local cortical network segregation. Trajectories represent the GAMM-predicted segregation values with a 95% credible interval band. **b,** The heterogenous patterning of the magnitude of age-by-disadvantage effects (F-statistic) on local segregation is shown on the cortical surface. Regions that show significant age-by-disadvantage effects passing FDR correction at p_{FDR} < 0.05 are outlined in black. **c,** Disadvantage associations with developmental increases in local segregation are enriched in sensorimotor systems. Boxplots show the magnitude of age-by-disadvantage effects; each point is an individual parcel (n = 286 parcels, excluding parcels with system assignment None). Boxplots show median and 25%-75% interquartile range; whiskers extend to 1.5 * interquartile range, points outside are shown as outliers.

We included a measure of pre-censoring motion, the total framewise displacement across all frames, instead of post-censoring motion, as a subject-level covariate. Global segregation ($F_{s(agexSES)}$ = 5.94, p = 0.003, p_{FDR} = 0.004), meso-scale segregation ($F_{s(agexSES)}$ = 9.70, p < 0.0001, p_{FDR} = 0.0002), and local segregation (Supplementary Figure 2a, $F_{s(agexSES)}$ = 13.17, p < 0.0001, p_{FDR} < 0.0001) all show significant and similar patterns of interactions, such that infants and toddlers with greater exposure to prenatal disadvantage show a faster increase in cortical network segregation than infants and toddlers with less disadvantage exposure. We did not find evidence for moderating associations of disadvantage with developmental changes in network integration ($F_{s(agexSES)}$ = 1.37, p = 0.255, p_{FDR} = 0.255). The magnitude of disadvantage associations with developmental increases in local segregation differed across functional

systems, with the strongest associations found in somatomotor-hand, somatomotor-mouth, dorsal attention, and frontoparietal systems (Supplementary Figure 2c).

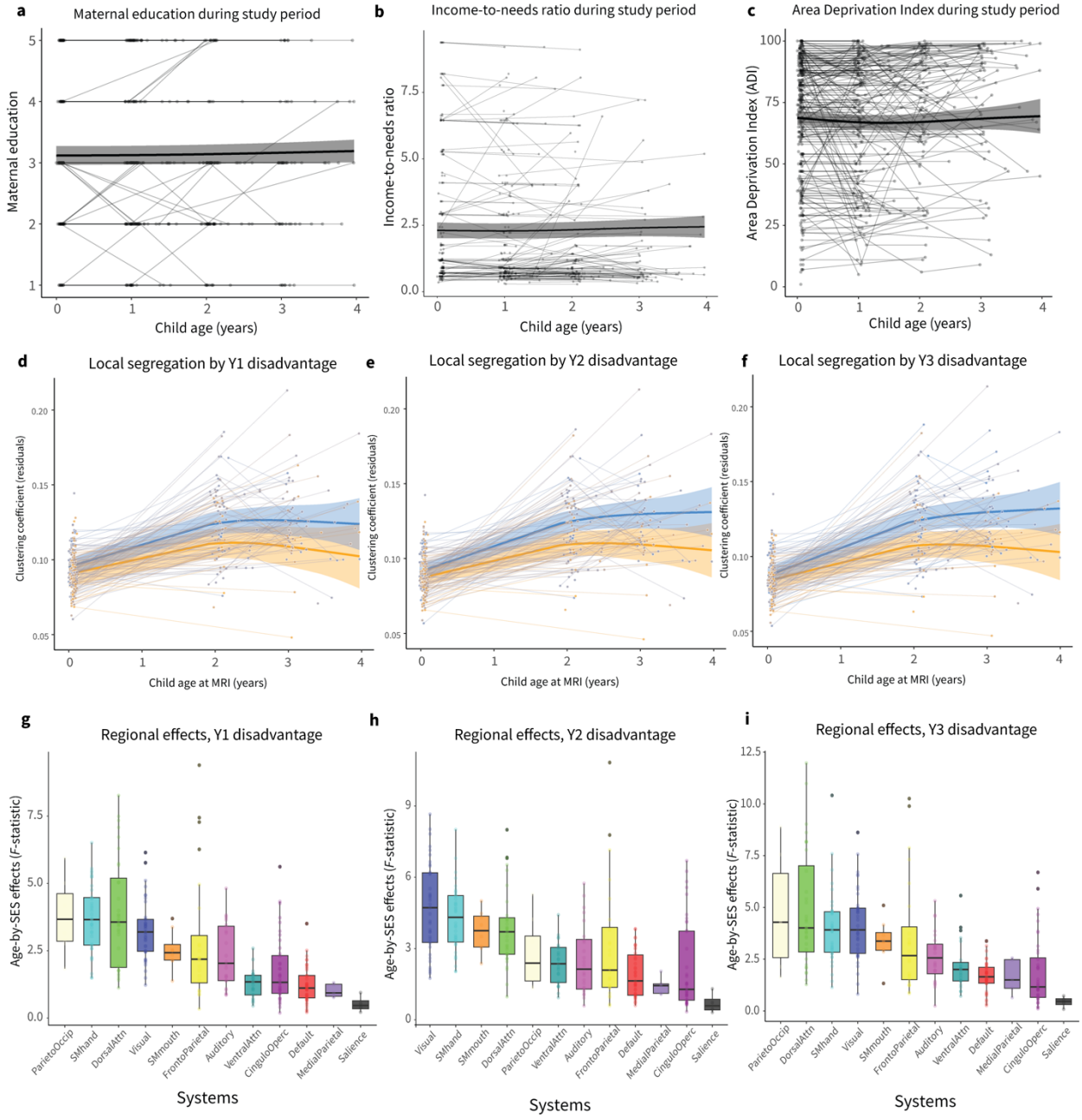

Supplementary Figure 3. Little evidence for changes in disadvantage during the study period. **a,** Maternal education does not change significantly over the study period. **b,** Income-to-needs ratio does not change significantly over the study period. **c,** Area deprivation index (ADI) does not change significantly over the study period. **d,** Year one disadvantage moderates trajectories of local cortical network segregation. **e,** Year two disadvantage moderates trajectories of local cortical network segregation. **f,** Year three disadvantage moderates trajectories of local cortical network segregation. **g,** Year one disadvantage associations with developmental increases in local segregation across functional systems. **h,** Year two disadvantage associations with

developmental increases in local segregation across functional systems. **i,** Year three disadvantage associations with developmental increases in local segregation across functional systems. Boxplots show the magnitude of age-by-disadvantage effects; each point is an individual parcel (n = 286 parcels, excluding parcels with system assignment None). Boxplots show median and 25%-75% interquartile range; whiskers extend to 1.5 * interquartile range, points outside are shown as outliers.

We first examined the extent of changes in concrete indicators of social disadvantage, finding that there was little evidence for social mobility during the study period: maternal education did not change significantly over time ($F_{s(\text{child age})} = 1.30$, EDF = 1.30, p = 0.358), nor did income-to-needs ratio ($F_{s(\text{child age})} = 1.01$, EDF = 1.62, p = 0.485), nor did neighborhood deprivation (ADI, $F_{s(\text{child age})} = 1.45$, EDF = 1.93, p = 0.193). We next examined whether our results were robust to using a disadvantage factor score from later timepoints, rather than the prenatal disadvantage factor score.

We find that across timepoints, global segregation ($F_{s(\text{agexSES\_y1})} = 2.72$, p = 0.067; $F_{s(\text{agexSES\_y2})} = 3.32$, p = 0.013; $F_{s(\text{agexSES\_y3})} = 6.785$, p = 0.001), meso-scale segregation ($F_{s(\text{agexSES\_y1})} = 4.19$, p = 0.016; $F_{s(\text{agexSES\_y2})} = 5.87$, p = 0.003; $F_{s(\text{agexSES\_y3})} = 7.56$, p < 0.001), and local segregation (Supplementary Figure 3d-f, $F_{s(\text{agexSES\_y1})} = 4.83$, p = 0.005; $F_{s(\text{agexSES\_y2})} = 8.71$, p < 0.001; $F_{s(\text{agexSES\_y3})} = 8.91$, p < 0.001) all show similar patterns of interactions, such that infants and toddlers with greater exposure to prenatal disadvantage show a faster increase in cortical network segregation than infants and toddlers with less disadvantage exposure. We found some evidence for moderating associations of disadvantage with developmental changes in network integration when using disadvantage factor scores from later timepoints ($F_{s(\text{agexSES\_y1})} = 2.22$, p = 0.039; $F_{s(\text{agexSES\_y2})} = 3.34$, p = 0.028; $F_{s(\text{agexSES\_y3})} = 2.43$, p = 0.028).

The magnitude of disadvantage associations with developmental increases in local segregation differed across functional systems, with the strongest associations found in somatomotor-hand, visual, somatomotor-mouth, dorsal attention, and parieto-occipital systems (Supplementary Figures 3g-i).

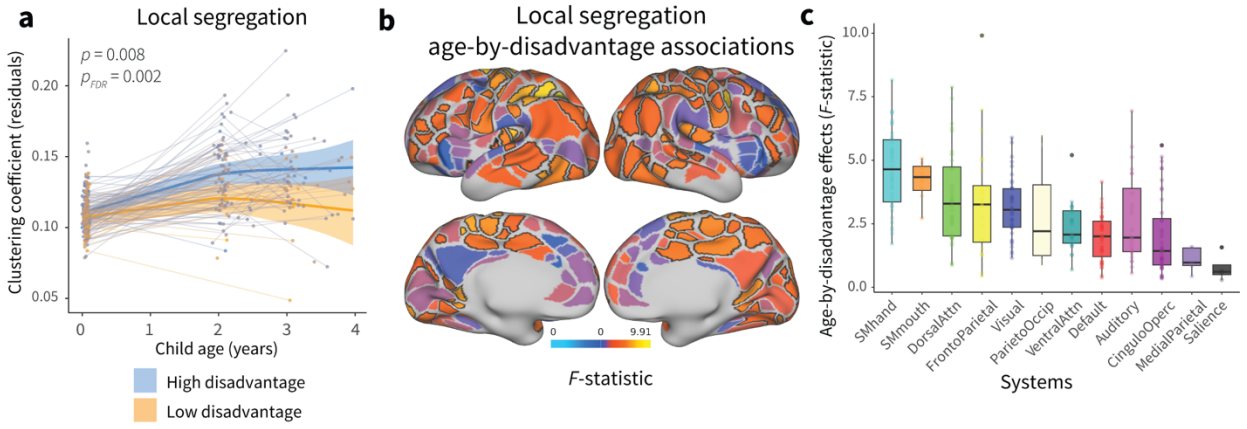

Supplementary Figure 4. Associations between the early environment and developmental increases in cortical network segregation, using a longitudinal mixed model including a random

slope for child age. **a,** Prenatal disadvantage moderates trajectories of local cortical network segregation. Trajectories represent the GAMM-predicted segregation values with a 95% credible interval band. **b,** The heterogenous patterning of the magnitude of age-by-disadvantage effects (F-statistic) on local segregation is shown on the cortical surface. Regions that show significant age-by-disadvantage effects passing FDR correction at $p_{FDR} < 0.05$ are outlined in black. **c,** Disadvantage associations with developmental increases in local segregation are enriched in sensorimotor systems. Boxplots show the magnitude of age-by-disadvantage effects; each point is an individual parcel (n = 286 parcels, excluding parcels with system assignment None). Boxplots show median and 25%-75% interquartile range; whiskers extend to 1.5 * interquartile range, points outside are shown as outliers.

In our main analyses, we examined longitudinal development of functional network architecture using generalized additive mixed models (GAMMs), where we included a random intercept per participant. Here we include both a random slope and a random intercept per participant (uncorrelated), and find that our results are qualitatively similar. Global segregation ($F_{s(agexSES)}$ = 3.83, p = 0.023, p_{FDR} = 0.030), meso-scale segregation ($F_{s(agexSES)}$ = 7.31, p < 0.001, p_{FDR} = 0.002), and local segregation (Supplementary Figure 4a, $F_{s(agexSES)}$ = 7.17, p = 0.008, p_{FDR} = 0.002) show similar patterns of interactions, such that infants and toddlers with greater exposure to prenatal disadvantage show a faster increase in cortical network segregation than infants and toddlers with less disadvantage exposure. There was a marginal moderating associations of disadvantage with developmental changes in network integration ($F_{s(agexSES)}$ = 2.49, p = 0.084, p_{FDR} = 0.084). The magnitude of disadvantage associations with developmental increases in local segregation differed across functional systems, with the strongest associations found in somatomotor-hand, somatomotor-mouth, dorsal attention, and frontoparietal systems (Supplementary Figure 4c).

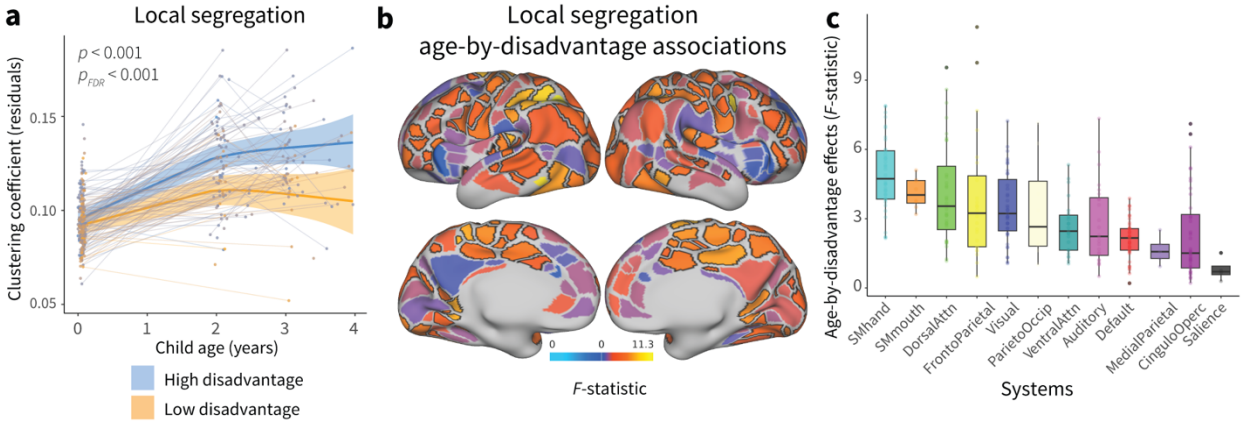

Supplementary Figure 5. Associations between the early environment and developmental increases in cortical network segregation, excluding outliers > 3 SD away from the mean. **a,** Prenatal disadvantage moderates trajectories of local cortical network segregation. Trajectories represent the GAMM-predicted segregation values with a 95% credible interval band. **b,** The heterogenous patterning of the magnitude of age-by-disadvantage effects (F-statistic) on local segregation is shown on the cortical surface. Regions that show significant age-by-disadvantage effects passing FDR correction at $p_{FDR} < 0.05$ are outlined in black. **c,**

Disadvantage associations with developmental increases in local segregation are enriched in sensorimotor systems. Boxplots show the magnitude of age-by-disadvantage effects; each point is an individual parcel (n = 286 parcels, excluding parcels with system assignment None). Boxplots show median and 25%-75% interquartile range; whiskers extend to 1.5 * interquartile range, points outside are shown as outliers.

We excluded outlier observations, that is, observations at a timepoint that were > 3 SD away from the mean, and find that our results are qualitatively similar. Global segregation ($F_{s(agexSES)}$ = 2.91, p = 0.052, p_{FDR} = 0.069), meso-scale segregation ($F_{s(agexSES)}$ = 7.68, p < 0.001, p_{FDR} = 0.001), and local segregation (Supplementary Figure 5a, $F_{s(agexSES)}$ = 13.32, p < 0.001, p_{FDR} < 0.001) show similar patterns of interactions, such that infants and toddlers with greater exposure to prenatal disadvantage show a faster increase in cortical network segregation than infants and toddlers with less disadvantage exposure. We found no evidence for moderating associations of disadvantage with developmental changes in network integration ($F_{s(agexSES)}$ = 1.862, p = 0.156, p_{FDR} = 0.156). The magnitude of disadvantage associations with developmental increases in local segregation differed across functional systems, with the strongest associations found in somatomotor-hand, somatomotor-mouth, dorsal attention, and frontoparietal systems (Supplementary Figure 5c).

Supplementary Note 2

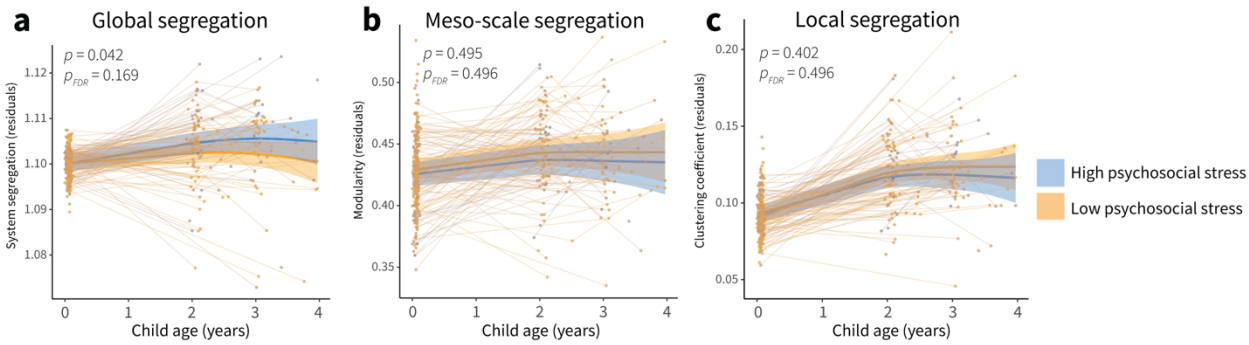

Supplementary Figure 6. Associations between prenatal psychosocial stress and developmental increases in cortical network segregation. **a,** Prenatal psychosocial stress moderates trajectories of global cortical network segregation. **b,** Prenatal psychosocial stress does not significantly moderate trajectories of meso-scale cortical network segregation. **c,** Prenatal psychosocial stress does not significantly moderate trajectories of local cortical network segregation. Plots display fitted network segregation trajectories from GAMM models plotted by age for participants from low psychosocial stress backgrounds (orange) and high psychosocial stress backgrounds (blue) with a 95% credible interval. Psychosocial stress was modeled continuously; for visualization purposes here we show model trajectories from lowest and highest deciles. Individual points represent individual scans, with lines indicating scans from the same participant.

As social disadvantage and psychosocial stress are moderately correlated at birth in our sample of children ($t(259) = 7.81$, $r = 0.436$, $p < 0.001$, 95% CI = [0.33, 0.53]), we investigated whether there were effects of psychosocial stress independent of disadvantage. Thus, we examined whether prenatal psychosocial stress was associated with measures of functional network architecture after controlling for prenatal disadvantage. We found that when controlling for the age-by-disadvantage interaction, global segregation shows an age-by-psychosocial stress interaction that does not pass FDR correction ($F_{s(agexSES)} = 3.19$, $p = 0.042$, $p_{FDR} = 0.169$), while meso-scale segregation ($F_{s(agexSES)} = 0.70$, $p = 0.495$, $p_{FDR} = 0.496$) and local segregation ($F_{s(agexSES)} = 0.91$, $p = 0.402$, $p_{FDR} = 0.496$) do not show even marginally significant interactions (Supplementary Figure 6). In all models, age-by-disadvantage interactions remain significant when including psychosocial stress in the model (p's < 0.05). We found no evidence for moderating associations of psychosocial stress with developmental changes in network integration when controlling for disadvantage ($F_{s(agexSES)} = 2.39$, $p = 0.093$, $p_{FDR} = 0.1986$).

Supplementary Table 1. Participant demographics at birth.

Variable	N = 261[1]
Age at scan (months)	41.3 (38.0 - 45.0)
Child race	
Black	156 / 261 (60%)
Chinese	2 / 261 (0.8%)
Multiracial	3 / 261 (1.1%)
Other	1 / 261 (0.4%)
Other Pacific Islander	1 / 261 (0.4%)
White	98 / 261 (38%)
Child ethnicity	
Not Hispanic or Latino	253 / 261 (97%)
Hispanic or Latino	6 / 261 (2.3%)
Unspecified	2 / 261 (0.8%)
Child sex	
Male	141 / 261 (54%)
Female	120 / 261 (46%)
Gestational age (weeks)	38.9 (37.0 - 41.6)
Birthweight (g)	3,274.0 (2,200.0 - 4,627.0)
Area Deprivation Index	67.5 (6.0 - 100.0)
Income to Needs Ratio	2.7 (0.4 - 9.4)
Highest level of parent education completed	
Less than 12th grade	22 / 251 (8.8%)
High school degree/GED	101 / 251 (40%)
Some college/vocational school	44 / 251 (18%)
College degree (4 years)	29 / 251 (12%)
Graduate degree	55 / 251 (22%)
Insurance status (private)	135 / 261 (52%)
Healthy Eating Index	58.7 (33.0 - 80.7)
Socioeconomic disadvantage factor score	-0.1 (-2.2 - 1.5)

[1]Mean (Range); n / N (%)

Supplementary Table 2. Bivariate correlations between disadvantage variables at birth.

	Area Deprivation Index (ADI)	*Income-to-Needs Ratio (INR)*	*Healthy Eating Index*	*Insurance status*	*Maternal education*
Area Deprivation Index (ADI)	1.00				
Income-to-Needs Ratio (INR)	-0.62***	1.00			
Healthy Eating Index	-0.28***	0.34***	1.00		
Insurance status (private/individual or public/uninsured)	-0.53***	0.67***	0.27***	1.00	
Maternal education	-0.61***	0.71***	0.40***	0.59***	1.00

*** $p < 0.001$

Spearman's correlation test, two-sided, was used to assess bivariate correlations. No multiple corrections adjustment was applied in this table.

Supplementary Table 3. Variables comprising the socioeconomic disadvantage factor at each timepoint.

Birth	Year 1	Year 2	Year 3
INR, 1st trimester	INR, 1 year	INR, 2 years	INR, 3 years
INR, 2nd trimester	Maternal education	Maternal education	Maternal education
INR, 3rd trimester	ADI at 4 months	ADI at 16 months	ADI at 28 months
Maternal education	ADI at 8 months	ADI at 20 months	ADI at 32 months
ADI at birth	ADI at 12 months	ADI at 24 months	ADI at 36 months
Insurance status			
Healthy Eating Index			

ADI: Area Deprivation Index, national percentile
INR: Income-to-needs ratio
Insurance status: private/individual or public/uninsured

Supplementary Table 4. Sample sizes for each set of timepoints

Birth only	Y2 only	Y3 only	Birth-Y2	Birth-Y3	Birth-Y2-Y3	Y2-Y3
160	13	3	42	26	33	4

Supplementary References

1. Gordon, E. M. *et al.* Generation and Evaluation of a Cortical Area Parcellation from Resting-State Correlations. *Cereb. Cortex N. Y. NY* **26**, 288–303 (2016).
2. Bassett, D. S., Zurn, P. & Gold, J. I. On the nature and use of models in network neuroscience. *Nat. Rev. Neurosci.* **19**, 566 (2018).
3. Zalesky, A., Fornito, A. & Bullmore, E. On the use of correlation as a measure of network connectivity. *NeuroImage* **60**, 2096–2106 (2012).
4. Lin, W. *et al.* Functional Connectivity MR Imaging Reveals Cortical Functional Connectivity in the Developing Brain. *AJNR Am. J. Neuroradiol.* **29**, 1883–1889 (2008).
5. Gao, W. *et al.* Evidence on the emergence of the brain's default network from 2-week-old to 2-year-old healthy pediatric subjects. *Proc. Natl. Acad. Sci.* **106**, 6790–6795 (2009).
6. Doria, V. *et al.* Emergence of resting state networks in the preterm human brain. *Proc. Natl. Acad. Sci.* **107**, 20015–20020 (2010).
7. Smyser, C. D. *et al.* Longitudinal Analysis of Neural Network Development in Preterm Infants. *Cereb. Cortex* **20**, 2852–2862 (2010).
8. Gao, W., Alcauter, S., Smith, J. K., Gilmore, J. & Lin, W. Development of human brain cortical network architecture during infancy. *Brain Struct. Funct.* **220**, 1173–1186 (2015).
9. Eyre, M. *et al.* The Developing Human Connectome Project: typical and disrupted perinatal functional connectivity. *Brain* **144**, 2199–2213 (2021).
10. Sylvester, C. M. *et al.* Network-specific selectivity of functional connections in the neonatal brain. *Cereb. Cortex* bhac202 (2022) doi:10.1093/cercor/bhac202.
11. Cole, M. W., Yarkoni, T., Repovš, G., Anticevic, A. & Braver, T. S. Global Connectivity of Prefrontal Cortex Predicts Cognitive Control and Intelligence. *J. Neurosci.* **32**, 8988–8999 (2012).
12. Bassett, D. S. & Bullmore, E. T. Small-world brain networks revisited. *The Neuroscientist* **23**, 499–516 (2017).
13. Good, B. H., de Montjoye, Y.-A. & Clauset, A. Performance of modularity maximization in practical contexts. *Phys. Rev. E* **81**, 046106 (2010).
14. Rubinov, M. & Sporns, O. Weight-conserving characterization of complex functional brain networks. *NeuroImage* **56**, 2068–2079 (2011).
15. Bassett, D. S., Nelson, B. G., Mueller, B. A., Camchong, J. & Lim, K. O. Altered resting state complexity in schizophrenia. *NeuroImage* **59**, 2196–2207 (2012).
16. Santarnecchi, E., Galli, G., Polizzotto, N. R., Rossi, A. & Rossi, S. Efficiency of weak brain connections support general cognitive functioning. *Hum. Brain Mapp.* **35**, 4566–4582 (2014).
17. Chan, M. Y., Park, D. C., Savalia, N. K., Petersen, S. E. & Wig, G. S. Decreased segregation of brain systems across the healthy adult lifespan. *Proc. Natl. Acad. Sci.* **111**, E4997–E5006 (2014).
18. Chan, M. Y. *et al.* Long-term prognosis and educational determinants of brain network decline in older adult individuals. *Nat. Aging* **1**, 1053–1067 (2021).
19. Porter, M. A., Onnela, J.-P. & Mucha, P. J. Communities in networks. *Not. AMS* **56**, 1082–1097 (2009).
20. Fortunato, S. Community detection in graphs. *Phys. Rep.* **486**, 75–174 (2010).
21. Newman, M. E. J. Modularity and community structure in networks. *Proc. Natl. Acad. Sci.* **103**, 8577–8582 (2006).
22. Achard, S., Salvador, R., Whitcher, B., Suckling, J. & Bullmore, E. A resilient, low-frequency, small-world human brain functional network with highly connected association cortical hubs. *J. Neurosci.* **26**, 63–72 (2006).
23. Bartolomei, F. *et al.* Disturbed functional connectivity in brain tumour patients: evaluation by graph analysis of synchronization matrices. *Clin. Neurophysiol.* **117**, 2039–2049 (2006).

24. Bassett, D. S., Meyer-Lindenberg, A., Achard, S., Duke, T. & Bullmore, E. Adaptive reconfiguration of fractal small-world human brain functional networks. *Proc. Natl. Acad. Sci.* **103**, 19518–19523 (2006).
25. Xu, T. *et al.* Network analysis of functional brain connectivity in borderline personality disorder using resting-state fMRI. *NeuroImage Clin.* **11**, 302–315 (2016).
26. Zhang, B. & Horvath, S. A general framework for weighted gene co-expression network analysis. *Stat. Appl. Genet. Mol. Biol.* **4**, 17 (2005).
27. Costantini, G. & Perugini, M. Generalization of clustering coefficients to signed correlation networks. *PLOS ONE* **9**, e88669 (2014).
28. Marek, S., Hwang, K., Foran, W., Hallquist, M. N. & Luna, B. The contribution of network organization and integration to the development of cognitive control. *PLOS Biol.* **13**, e1002328 (2015).
29. Sanders, A. F. P. *et al.* Age-related differences in resting-state functional connectivity from childhood to adolescence. *Cereb. Cortex* bhad011 (2023) doi:10.1093/cercor/bhad011.
30. Baum, G. L. *et al.* Modular segregation of structural brain networks supports the development of executive function in youth. *Curr. Biol.* **27**, 1561–1572 (2017).
31. Rubinov, M. & Sporns, O. Complex network measures of brain connectivity: Uses and interpretations. *NeuroImage* **52**, 1059–1069 (2010).